

Superconductivity of CH₄-intercalated H₃S under high pressure

Mingyang Du¹, Zihan Zhang¹, Tian Cui^{2,1,*}, Defang Duan^{1,*}

¹ College of Physics, Jilin University, Changchun 130012, People's Republic of China

² Institute of High Pressure Physics, School of Physical Science and Technology, Ningbo University, Ningbo, 315211, People's Republic of China

KEYWORDS: Hydrides, High pressure, Superconductivity, first principles calculation.

ABSTRACT

The discovery of the high temperature superconducting state in compounds of hydrogen, carbon and sulfur with the critical temperature (T_c) of 288 K at high pressure is an important milestone towards room-temperature superconductors. Here, we have extensively investigated the high-pressure phases of CS_2H_{10} , and found four phases $Cmc2_1$, $P3m1$, $P-3m1$ and Pm . Among them, $P3m1$ can be dynamically stable at pressure as low as 50 GPa, and $Cmc2_1$ has high T_c of 155 K at 150 GPa. Both of $Cmc2_1$ and $P3m1$ are host-guest hydrides, in which CH_4 molecules are inserted into $Im-3m\text{-H}_3\text{S}$ and $R3m\text{-H}_3\text{S}$ sublattices, respectively. Their T_c is dominated by the H_3S lattice inside. The insertion of CH_4 greatly reduces the pressure required for the stability of the original H_3S lattice, but it has a negative impact on superconductivity that cannot be ignored. By studying the effect of CH_4 insertion in the H_3S lattice, we can design hydrides with T_c close to that of H_3S and a greatly reduced pressure required for stability.

Introduction

In the Ginzburg's list of "especially important and interesting problems"¹, room temperature superconductivity and metallic hydrogen ranked second and third, respectively. Both problems have attracted solid physicists for decades. In recent years, these problems seem to have a common solution: high-pressure hydrides. According to BCS theory², the high superconducting transition temperature (T_c) requires higher electronic density of states and phonon frequencies near the Fermi level. Metallic hydrogen formed under high pressure is expected to be a high temperature superconductor because of large vibration frequency^{3, 4}, but theoretical and experimental results show that metallic hydrogen requires extremely high pressure^{5, 6}. Hydrogen-rich compounds can be an alternative way to find high-temperature superconductors, because the "chemical pre-compression" greatly reduces the metallization pressure^{7, 8}.

Theoretical investigations have predicted that H₃S is a high temperature superconductor with T_c of about 200 K at high pressure^{9, 10}, which has been confirmed by experiments, with the T_c of 203 K^{11, 12}. This observation indicates the feasibility of finding high T_c in hydrogen-rich materials, attracting people to quest more hydrogen-rich superconductors under high pressure. Metal hydrides have been the focus of research¹³⁻²¹. Some of them have been experimentally confirmed, such as LaH₁₀^{22, 23}, YH₆²⁴, YH₉²⁵, CaH₆²⁶ and ThH₁₀²⁷. Recently, Snider et al. observed the high- T_c state with 288 K in compounds of hydrogen, carbon and sulfur at pressure of 267 GPa, which is a milestone towards room-temperature superconductors²⁸. Unfortunately, its stoichiometry and crystal structure are still uncertain. In fact, not only this room temperature superconducting phase, the entire structural evolution of C-S-H system under high pressure are lack, which makes subsequent research difficult. Therefore, investigation of the stoichiometry

and structural evolution of C-S-H system is necessary to provide useful complementary information for experimental observation.

When Li et al. studied $Pm-3m$ -H₃SXe with a similar structure to $Im-3m$ -H₃S, they found that the "H₃S" host lattice is a key factor affecting the T_c ²⁹. Therefore, the room temperature superconducting C-S-H compound was considered to be C-doped H₃S for a period of time. Later, Ge et al. did find that 3.8% C (H₃S_{0.962}C_{0.038}) can raise the T_c of H₃S to 289 K at 260 GPa³⁰. However, the recent two experiments on the high-pressure structure and composition of the C-S-H system reported that its structure is complex and different from the common $Im-3m$ -H₃S^{31, 32}. According to the experimental data, the C-S-H compound should be much richer in hydrogen than H₃S. A metastable hydrogen-rich host-guest CSH₇ compound with similar structures $I-43m$, Cm , $R3m$, and $Pnma$ were found before, where C and H form methane molecules CH₄ which was inserted into the H₃S sublattice³³. The electron-phonon coupling calculations reveal superconductivity with T_c 's as high as 194 K at 150 GPa³⁴. Most recently, Wang et al. studied the C-S-H system more extensively³⁵ and believe that the structure containing more carbon and hydrogen is unlikely to be a low-enthalpy phase and easily decomposes into H₂, H₃S, or CH_x. In the ternary structures they explored, only CS₂H₁₀ has a lower enthalpy (-65 meV/atom).

Here, we have extensively investigated the high-pressure phases of CS₂H₁₀ and found $Cmc2_1$, $P3m1$, $P-3m1$ and Pm phases. The $Cmc2_1$ is a host-guest structure in which CH₄ molecules are inserted into the H₃S sublattice, which is a potential high-temperature superconductor with T_c of 155 K at 150 GPa. The H₃S lattice makes a decisive contribution to superconductivity, and the CH₄ molecules in the middle of the H₃S sublattice can greatly reduce the pressure required for the stability of the H₃S lattice. This discovery can not only help us further understand the

evolution process of the C-S-H system within 50-200 GPa, but also provide useful guidance on how to reduce the stable pressure of high-temperature superconducting hydrides.

Computational details

Ab initio random structure searching (AIRSS) technique^{36, 37} and ab initio calculation of the Cambridge Serial Total Energy Package (CASTEP)³⁸ were used to predict the candidate crystal structures of CS₂H₁₀. The plane-wave cut-off energy of 300 eV and the Brillouin zone sampling grid spacing of $2\pi \times 0.07 \text{ \AA}^{-1}$ were selected. The generalized gradient approximation (GGA) with the Perdew-Burke-Ernzerhof (PBE) parametrization³⁹ for the exchange-correlation functional and on-the-fly (OTF) generation of ultra-soft potentials were used for the structure searching.

The Vienna ab initio simulation program (VASP)⁴⁰ was used for structural relaxation and calculations of enthalpies and electronic properties. The projector augmented plane-wave (PAW) potentials⁴¹ with an energy cutoff of 1000 eV and Monkhorst-Pack (MP)⁴² meshes for Brillouin zone sampling with resolutions of $2\pi \times 0.03 \text{ \AA}^{-1}$ were used to ensure that all enthalpy calculations are well converged to less than 1 meV per atom.

The Quantum-ESPRESSO⁴³ was used in phonon and electron-phonon calculations. Ultra-soft potentials were used with a kinetic energy cut-off of 90 Ry. The k-points and q-points meshes in the first Brillouin zone are $9 \times 9 \times 9$ and $3 \times 3 \times 3$ for *Cmc2₁*, $9 \times 9 \times 15$ and $3 \times 3 \times 5$ for *P3m1*, $9 \times 9 \times 15$ and $3 \times 3 \times 5$ for *P-3m1*, $6 \times 8 \times 12$ and $2 \times 4 \times 4$ for *Pm*. The superconducting transition temperatures of these structures are estimated through the Allen-Dynes-modified McMillan equation (A-D-M) with correction factors^{44, 45} and self-consistent solution of the Eliashberg equation (scE)⁴⁶.

Results and discussion

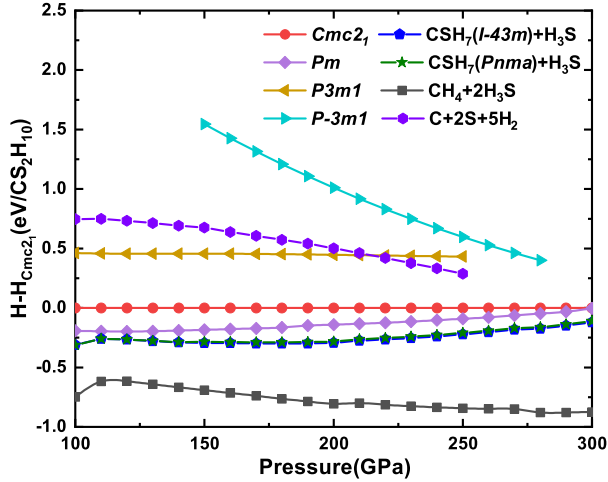


Fig. 1. Calculated enthalpies per CS_2H_{10} unit as the function of pressure for our predicted candidate structures, CSH_7 ($I-43m$ ³³ and $Pnma$ ³⁴) + H_3S ($Cccm$, $R3m$ and $Im-3m$ ⁹), molecular assemblage CH_4 ($Cmcm$ and $Pnma$ ⁴⁷) + $2\text{H}_3\text{S}$, and the assemblage C ($Fd-3m$ ⁴⁸) + 2S (β - Po ⁴⁹) + 5H_2 ($P6_3/mc$, $C2/c$ and $Cmca$ -12⁵⁰) relative to the $Cmc2_1$ phase.

We performed detailed structure searches focusing on CS_2H_{10} with 1 to 4 formula units at pressure of 100-300 GPa. Four new structures are uncovered: $Cmc2_1$, $P3m1$, $P-3m1$ and Pm , and their enthalpy curves are shown in Fig. 1. The Pm and $Cmc2_1$ phase emerged as being stable relative to the elements in the pressure range considered, but their enthalpy is higher than $\text{CH}_4 + 2\text{H}_3\text{S}$, and slightly higher than $\text{CSH}_7 + \text{H}_3\text{S}$. The calculation of the phonon spectrum shows that $P3m1$ can be dynamically stable at a pressure as low as 50 GPa. When the pressure exceeds 220 GPa, its energy is higher than the elemental substance and begins to decompose. The enthalpy of $P-3m1$ is much higher than other phases at 150 GPa, but its enthalpy decreases rapidly as the pressure increases, it may be more stable than other structures at pressures above 300 GPa. Then, we calculated the phonon spectrum of these structures at different pressures (see Fig. S1). As a result, there are no imaginary frequency modes in the entire Brillouin zone, which proves the

dynamic stability of all four structures. It is expected that these phases could be realized experimentally.

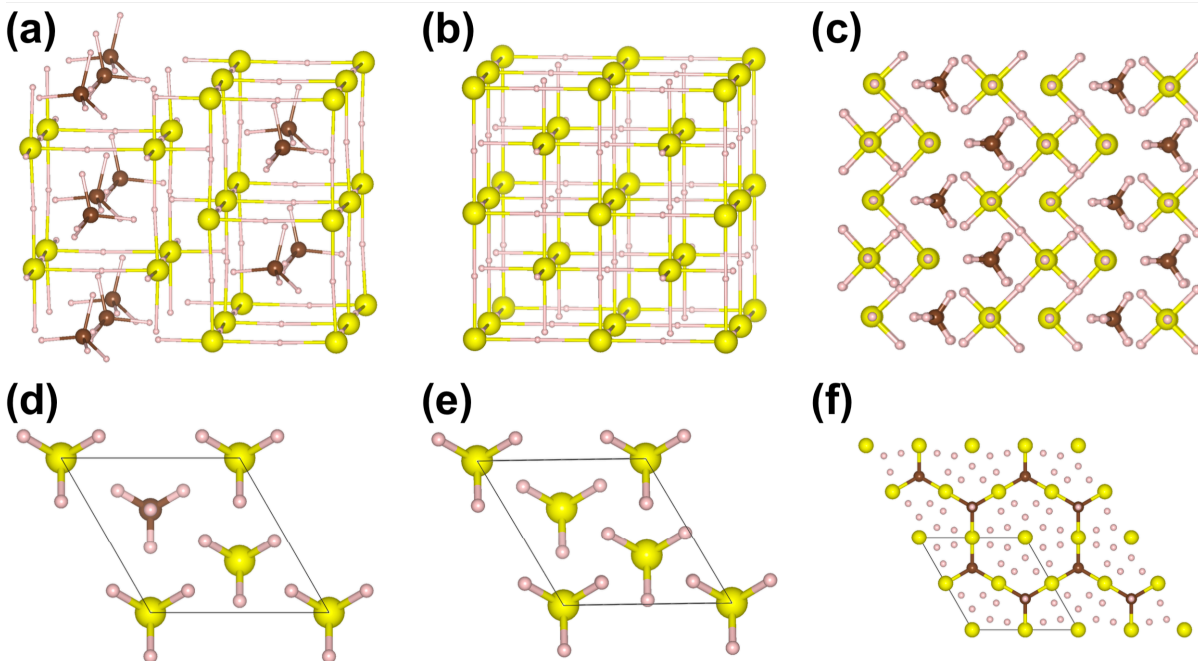


Fig. 2. (a) $Cmc2_1$ - CS_2H_{10} at 150 GPa, (b) $Im-3m$ - H_3S at 200 GPa, (c) Pm - CS_2H_{10} at 200 GPa, (d) $P3m1$ - CS_2H_{10} at 50 GPa, (e) $R3m$ - H_3S at 130 GPa and (f) $P-3m1$ - CS_2H_{10} at 100 GPa. The brown, yellow, and pink spheres denote C, S, and H atoms, respectively.

The predicted crystal structures of CS_2H_{10} are shown in Fig. 2, and their structure parameters are listed in Table S1 of the supplementary information. The $Im-3m$ - H_3S is characterized by S atoms located at a simple body-centered cubic lattice (bcc) and H atoms located symmetrically between S atoms. From Fig. 2a and b, it can be seen that the H_3S in $Cmc2_1$ has the same lattice as $Im-3m$ - H_3S , with slight distortion. The regular octahedron SH_6 in $Im-3m$ - H_3S was replaced with CH_4 , which is similar to the previously reported CSH_7 . The structure of Pm is also formed by inserting CH_4 molecules into the H_3S lattice, except that the replacement position of CH_4 is different from $Cmc2_1$ (see Fig. 2c). The $P3m1$ phase is composed of CH_4 molecules and SH_3 molecules, and the arrangement of SH_3 molecules is the same as that of $R3m$ - H_3S (see Fig. 2d

and e). The structure of $P-3m1$ is composed of CS_2 pleated hexagonal framework and hydrogen atoms (see Fig. 2f).

Table 1. The calculated EPC parameter (λ), logarithmic average phonon frequency (ω_{\log}), superconducting critical temperature $f_1 f_2 T_c$ using Allen-Dynes modified McMillan equation and T_c^{scE} using the Self-consistent solution of the Eliashberg equation.

Phase	Pressure (GPa)	λ	ω_{\log} (K)	$f_1 f_2 T_c$ (K)	T_c^{scE} (K)
$Cmc2_1$	150	2.01	799	128-141	142-155
$P3m1$	50	1.51	651	77-86	85-95
$P3m1$	100	1.21	916	79-90	84-95
$P-3m1$	100	0.63	1113	22-31	22-30
Pm	200	0.69	1386	36-47	39-50

the Coulomb pseudopotential $\mu^* = 0.10$ and 0.13 .

To examine the superconductivity in predicted four structures of CS_2H_{10} , we calculate the electron-phonon coupling constant (λ) and average phonon frequency (ω_{\log}) as shown in Table S5. For $Cmc2_1$, λ can reach 2.01 indicating that it is a strong electron-phonon coupling superconductor. But the λ of $Cmc2_1\text{-CS}_2\text{H}_{10}$ is lower than that of $I-43m\text{-CSH}_7$ ($\lambda = 3.64$ at 100 GPa), $Pnma\text{-CSH}_7$ ($\lambda = 3.06$ at 150 GPa), $R3m\text{-CSH}_7$ ($\lambda = 2.47$ at 150 GPa³⁴) and $Im-3m\text{-H}_3\text{S}$ ($\lambda = 2.19$ at 200 GPa), which is not beneficial for superconductivity. The logarithmic average phonon frequency ($\omega_{\log} = 799$ K) of $Cmc2_1\text{-CS}_2\text{H}_{10}$ is higher than that of $I-43m\text{-CSH}_7$ ($\omega_{\log} = 395$ K) and $Pnma\text{-CSH}_7$ ($\omega_{\log} = 672$ K). Furthermore, we estimated the T_c of $Cmc2_1$ to be 128 - 141 K at 150 GPa using Allen-Dynes modified McMillan equation⁴⁵ with typical values of the Coulomb pseudopotential $\mu^* = 0.13 - 0.1$. The calculation of the phonon spectrum shows that $P3m1$ can be dynamically stable at a pressure as low as 50 GPa, with T_c of 85-95 K. The T_c of $P-3m1$ and Pm is relatively low (< 100 K), as shown in Table 1. To better describe the systems with strong electron-phonon coupling (i.e., for $\lambda > 1.5$), we evaluate the T_c of these structures by the self-consistent solution of the Eliashberg equation⁴⁶. The T_c of $Cmc2_1$ can reach 142-155 K at

150 GPa, which is close to the T_c of C-S-H compound at 150 GPa measured by Snider et al. in the experiment²⁸. However, the gap between CS₂H₁₀ and C-S-H compounds rapidly increases in the higher pressure range. Except for $Cmc2_1$ with a larger λ , the T_c of other phases did not increase significantly.

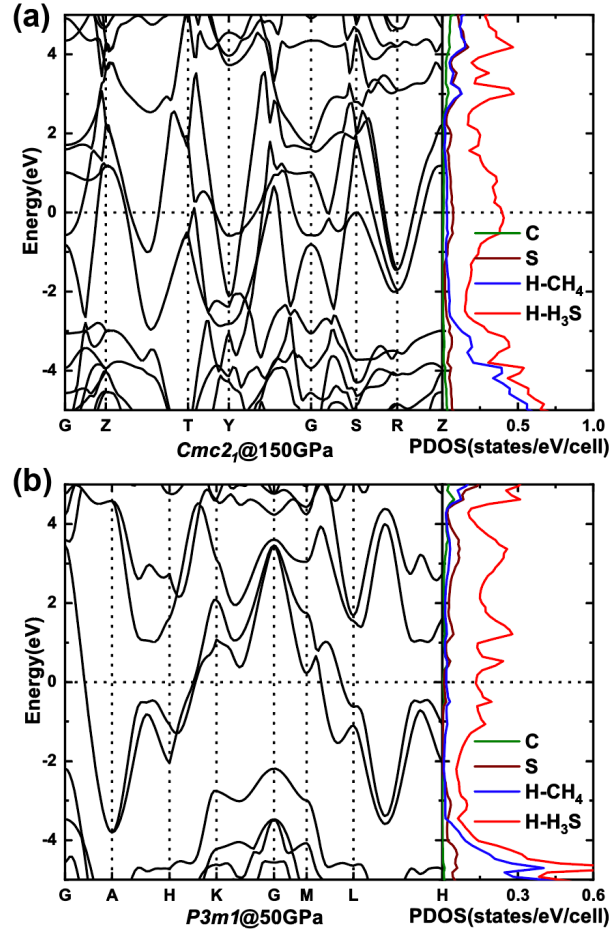


Fig. 3. Electronic band structure and projected density of states (PDOS) of (a) $Cmc2_1$ at 150 GPa and (b) $P3m1$ at 50 GPa.

In order to further explore the origin of superconductivity in $Cmc2_1$ and $P3m1$, we calculated their electronic properties. The electronic band structure shows that they are all metallic phases (see Fig. 3). It can be seen that the decisive contribution near the Fermi surface is the H in the

H₃S lattice, and the H in CH₄ contribute only to the deep energy levels (< -3 eV). Unlike H₃S, S in CS₂H₁₀ contributes little to the Fermi surface, which is unfavorable for the superconductivity of covalent hydrides. Therefore, in these two types of CS₂H₁₀, the superconductivity is driven by H on H₃S, and the insertion of CH₄ affects the strong hybridization of the orbitals of S and H atoms, resulting in a decrease in T_c .

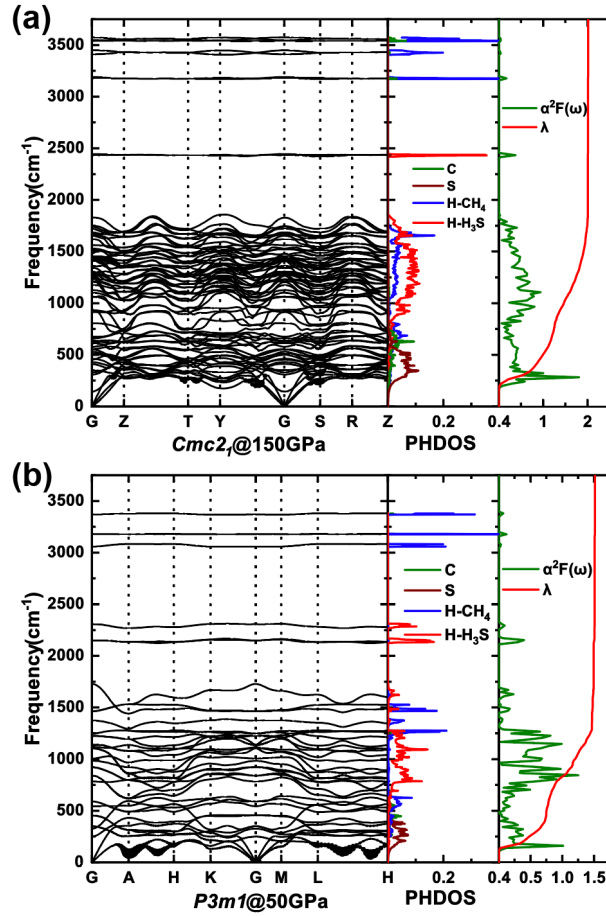


Fig. 4. Phonon dispersion curves, phonon density of states (PHDOS) projected on C, S, H in CH₄ and H in H₃S, and Eliashberg spectral function $\alpha^2F(\omega)$ together with the electron-phonon integral λ for (a) *Cmc2*₁ at 150 GPa and (b) *P3m1* at 50 GPa.

By comparing the electron-phonon integral λ of H₃S (see right panel of Fig. 5 in ref.⁹) and CS₂H₁₀ (see right panel of Fig. 4a and b), we can find that the contribution of S in the low

frequency region ($< 700 \text{ cm}^{-1}$) to λ is basically the same. The decrease of λ in CS_2H_{10} is mainly due to the decrease in the contribution of H on the H_3S in the middle frequency region. The phonons in the high frequency region ($> 3000 \text{ cm}^{-1}$) mainly come from H on CH_4 , which is consistent with CSH_7 . Compared to CSH_7 , CS_2H_{10} has an additional peak contributed by H on H_3S in $2000 - 2500 \text{ cm}^{-1}$ region. In $Cmc2_1$, this peak corresponds to the two H on the H_3S closest to CH_4 (see H3 in Fig. 5a). The insertion of CH_4 breaks the S-H bond on one side, so they only connect one S atom, and their frequency is higher than the frequency of the H connecting two S atoms (H2). In $P3m1$, this peak corresponds to the three H on the H_3S closest to CH_4 (see H3 in Fig. 5b). The insertion of CH_4 break the original S-H bond, and increase the frequency of the surrounding H (H3). Therefore, in these two types of CS_2H_{10} , the insertion of CH_4 affects the surrounding H on the H_3S (H3), which weakens its effect on electron-phonon coupling, and only H protected by two S-H covalent bonds (H2) makes a major contribution to superconductivity. This is the reason why the T_{cS} of $Cmc2_1\text{-CS}_2\text{H}_{10}$ and $P3m1\text{-CS}_2\text{H}_{10}$ are lower than that of $Im\text{-}3m\text{-H}_3\text{S}$ and $R3m\text{-H}_3\text{S}$. The CH_4 in $R3m\text{-CSH}_7$ does not destroy the original S-H bond, and the surrounding H on the H_3S (H2) is well protected by two S-H bonds³⁴. So, the T_c of $R3m\text{-CSH}_7$ can be as high as 181 - 191 K, which is very close to $Im\text{-}3m\text{-H}_3\text{S}$ (191 - 204 K). Therefore, in the future, when inserting CH_4 to reduce the pressure required for the stability of the H_3S system, special attention should be paid to the position of CH_4 insertion, which will have a great impact on T_c .

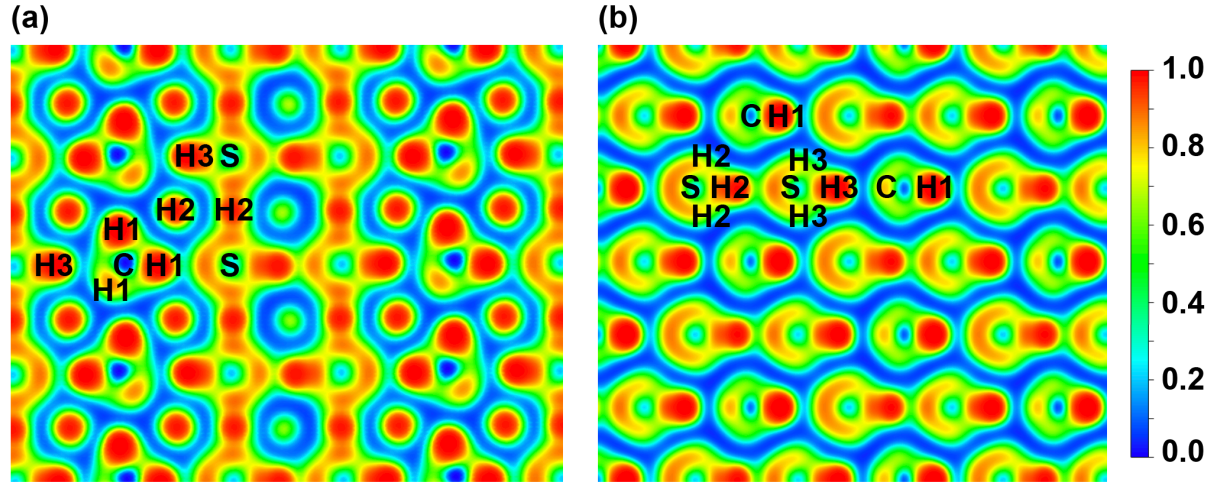


Fig. 5. Calculated electronic localization functions (ELF) of (a) $Cmc2_1$ at 150 GPa and (b) $P3m1$ at 50 GPa. H1 is the H on CH_4 , and H2 is the H farther from CH_4 on H_3S . H3 is the H on H_3S that is closer to CH_4 .

To explore the bonding in the $Cmc2_1$ and $P3m1$ phases, their ELF's were plotted in Fig. 5. The ELF is useful for visualizing covalent bonds and lone pairs; it maps values in the range from 0 to 1, where 1 corresponds to perfect localization of the valence electrons indicative of a strong covalent bond. In $Cmc2_1$, the ELF value inside the H_3S lattice is between 0.8-0.9, which has strong covalent properties like $Im-3m-H_3S$. However, the ELF value around CH_4 is close to 0, and it can only reach 0.4 between the nearest S atom, which is closer to the ELF value of the ionic bond. By comparing the ELF of $Cmc2_1$ (see Fig. 5a) and $Im-3m-H_3S$ (see Fig. 6d in Ref.⁹), we can find that the insertion of CH_4 does not affect H2 with two S-H bonds. But for H3, where one of the S-H bonds is broken, their charge density increases. By comparing the ELF of $P3m1$ (see Fig. 5b) and $R3m-H_3S$ (see Fig. 6b in Ref.⁹), we can also find that H3, which is closer to CH_4 , has a more localized charge, while the charge distribution of H2 is similar to that of H in $R3m-H_3S$. Although this change caused by CH_4 is detrimental to superconductivity, it can make the H_3S lattice stable at lower pressures. The volume of CS_2H_{10} changes more with pressure than

H₃S (see Fig. 6). A smaller volume means a smaller PV term under high pressure which in turn means a lower enthalpy. The insertion of CH₄ breaks the isotropy of H₃S. The H₃S lattice in CS₂H₁₀ still maintains the same properties as H₃S, but some H atoms were driven away from their symmetric positions to asymmetric ones in H₃S lattice due to the anisotropic interaction between the CH₄ and H₃S lattices. The lattice distortion caused by the movement of H atoms make CS₂H₁₀ more adaptable to pressure changes than H₃S. This is also the same in *I*-43m-CSH₇³³.

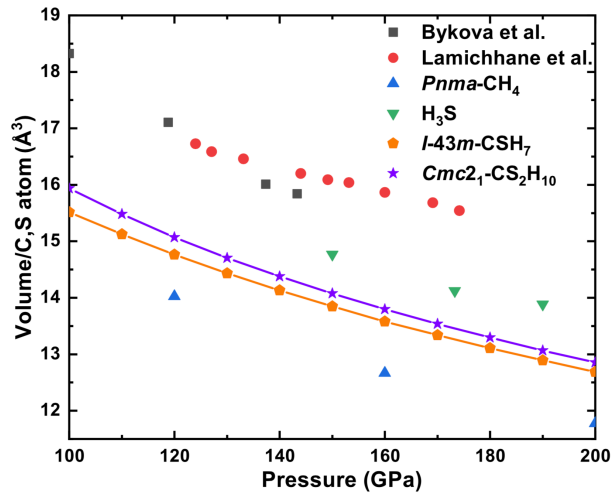


Fig. 6. Pressure-volume (P-V) relations measured for CS₂H₁₀ (*Cmc2*₁) compared to C-S-H compounds^{31, 32}, H₃S¹², CH₄⁴⁷ and CSH₇ (*I*-43m)^{33, 34}.

Due to the larger crystal lattice of H₃S, CS₂H₁₀ with more S has a larger volume than CSH₇. However, the volume of the experimentally synthesized C-S-H compound far exceeds that of CSH₇, CS₂H₁₀, or even H₃S, which means that the experimentally obtained structure is unlikely to be CH₄ insertion H₃S or doped H₃S structure. It is necessary to find a structure consistent with the experiment from more hydrogen-rich phases.

Conclusions

We searched for the crystal structures of the CS_2H_{10} by random structure searching up to 300 GPa. Four new and metastable phases $Cmc2_1$, $P3m1$, $P-3m1$ and Pm were uncovered, which are all metallic and show superconducting properties. The $P3m1$ phase can be dynamically stable at much lower pressure of 50 GPa with T_c of 155 K. For $Cmc2_1$ phase, it has high T_c of 155 K at 150 GPa. The insertion of CH_4 greatly reduces the pressure required for the stability of the original H_3S lattice, but it also has a negative impact on superconductivity that cannot be ignored. By comparing the experimental P-V diagram, we think that the phase obtained by the experiment is neither CH_4 insertion H_3S nor doped H_3S . The C-S-H compound in the experiment should be found from a more hydrogen-rich area.

Author Contributions

Defang Duan and Tian Cui directed the study. Mingyang Du conceived and performed the main work. All authors reviewed the paper.

Conflict of interest

The authors declare no competing financial interest.

ACKNOWLEDGMENT

This work was supported by the National Natural Science Foundation of China (Nos. 11674122, 51632002 and 52072188). Parts of calculations were performed in the High Performance Computing Center (HPCC) of Jilin University and TianHe-1(A) at the National Supercomputer Center in Tianjin.

REFERENCES

1. V. L. Ginzburg, *Uspekhi Fiz. Nauk*, 1999, **169**, 419–441.
2. J. Bardeen, L. N. Cooper and J. R. Schrieffer, *Phys. Rev.*, 1957, **106**, 162–164.
3. E. Wigner and H. B. Huntington, *The Journal of Chemical Physics*, 1935, **3**, 764–770.
4. J. M. McMahon and D. M. Ceperley, *Phys. Rev. B*, 2012, **85**.
5. J. M. McMahon, M. A. Morales, C. Pierleoni and D. M. Ceperley, *Rev. Mod. Phys.*, 2012, **84**, 1607–1653.
6. R. P. Dias and I. F. Silvera, *Science*, 2017, **355**, 715–718.
7. N. W. Ashcroft, *Phys. Rev. Lett.*, 2004, **92**, 4.
8. J. J. Gilman, *Phys. Rev. Lett.*, 1971, **26**, 546–548.
9. D. F. Duan, Y. X. Liu, F. B. Tian, D. Li, X. L. Huang, Z. L. Zhao, H. Y. Yu, B. B. Liu, W. J. Tian and T. Cui, *Sci Rep*, 2014, **4**, 6.
10. D. F. Duan, X. L. Huang, F. B. Tian, D. Li, H. Y. Yu, Y. X. Liu, Y. B. Ma, B. B. Liu and T. Cui, *Phys. Rev. B*, 2015, **91**, 5.
11. A. P. Drozdov, M. I. Eremets, I. A. Troyan, V. Ksenofontov and S. I. Shylin, *Nature*, 2015, **525**, 73–+.
12. M. Einaga, M. Sakata, T. Ishikawa, K. Shimizu, M. I. Eremets, A. P. Drozdov, I. A. Troyan, N. Hirao and Y. Ohishi, *Nat. Phys.*, 2016, **12**, 835–838.
13. H. Wang, J. S. Tse, K. Tanaka, T. Iitaka and Y. Ma, 2012, **109**, 6463.
14. X. Feng, J. Zhang, G. Gao, H. Liu and H. Wang, *RSC Adv.*, 2015, **5**, 59292–59296.
15. Y. Li, J. Hao, H. Liu, J. S. Tse, Y. Wang and Y. Ma, 2015, **5**, 9948.
16. K. Abe, 2017, **96**, 144108.
17. M. Du, Z. Zhang, H. Song, H. Yu, T. Cui, V. Z. Kresin and D. Duan, *Phys. Chem. Chem. Phys.*, 2021, **23**, 6717–6724.
18. H. Xie, Y. Yao, X. Feng, D. Duan, H. Song, Z. Zhang, S. Jiang, S. A. T. Redfern, V. Z. Kresin, C. J. Pickard and T. Cui, *Phys. Rev. Lett.*, 2020, **125**, 217001.
19. X.–H. Xiao, D.–F. Duan, Y.–B. Ma, H. Xie, H. Song, D. Li, F.–B. Tian, B.–B. Liu, H.–Y. Yu and T. Cui, *Frontiers of Physics*, 2019, **14**, 43601.
20. Y. X. Liu, D. F. Duan, F. B. Tian, C. Wang, Y. B. Ma, D. Li, X. L. Huang, B. B. Liu and T. Cui, *Phys. Chem. Chem. Phys.*, 2016, **18**, 1516–1520.
21. E. Zurek and W. Grochala, *Phys. Chem. Chem. Phys.*, 2015, **17**, 2917–2934.
22. M. Somayazulu, M. Ahart, A. K. Mishra, Z. M. Geballe, M. Baldini, Y. Meng, V. V. Struzhkin and R. J. Hemley, *Phys. Rev. Lett.*, 2019, **122**, 6.
23. A. P. Drozdov, P. P. Kong, V. S. Minkov, S. P. Besedin, M. A. Kuzovnikov, S. Mozaffari, L. Balicas, F. F. Balakirev, D. E. Graf, V. B. Prakapenka, E. Greenberg, D. A. Knyazev, M. Tkacz and M. I. Eremets, *Nature*, 2019, **569**, 528–+.
24. I. A. Troyan, D. V. Semenov, A. G. Kvashnin, A. G. Ivanova, V. B. Prakapenka, E. Greenberg, A. G. Gavriliuk, I. S. Lyubutin, V. V. Struzhkin and A. R. Oganov, in *arXiv e-prints* 2019, p. arXiv:1908.01534.
25. P. P. Kong, V. S. Minkov, M. A. Kuzovnikov, S. P. Besedin, A. P. Drozdov, S. Mozaffari, L. Balicas, F. F. Balakirev, V. B. Prakapenka, E. Greenberg, D. A. Knyazev and M. I. Eremets, in *arXiv e-prints* 2019, p. arXiv:1909.10482.
26. L. Ma, K. Wang, Y. Xie, X. Yang, Y. Wang, M. Zhou, H. Liu, G. Liu, H. Wang and Y. Ma, Experimental observation of superconductivity at 215 K in calcium superhydride under high pressures, 2021.

27. D. V. Semenov, A. G. Kvashnin, A. G. Ivanova, V. Svitlyk, V. Y. Fomin, A. V. Sadakov, O. A. Sobolevskiy, V. M. Pudalov, I. A. Troyan and A. R. Oganov, *Mater. Today*, 2020, **33**, 36–44.
28. E. Snider, N. Dasenbrock-Gammon, R. McBride, M. Debessai, H. Vindana, K. Vencatasamy, K. V. Lawler, A. Salamat and R. P. Dias, *Nature*, 2020, **586**, 373–377.
29. D. Li, Y. Liu, F. –B. Tian, S. –L. Wei, Z. Liu, D. –F. Duan, B. –B. Liu and T. Cui, *Frontiers of Physics*, 2018, **13**, 137107.
30. Y. Ge, F. Zhang, R. P. Dias, R. J. Hemley and Y. J. a. e.–p. Yao, 2020, p. arXiv:2011.12891.
31. E. Bykova, M. Bykov, S. Chariton, V. B. Prakapenka, K. Glazyrin, A. Aslandukov, A. Aslandukova, G. Criniti, A. Kurnosov and A. F. Goncharov, *Phys. Rev. B*, 2021, **103**, L140105.
32. A. Lamichhane, R. Kumar, M. Ahart, N. Salke, N. Dasenbrock-Gammon, E. Snider, Y. Meng, B. Lavina, S. Chariton, V. B. Prakapenka, M. Somayazulu, R. P. Dias and R. J. J. a. e.–p. Hemley, 2021, p. arXiv:2105.06352.
33. Y. Sun, Y. F. Tian, B. W. Jiang, X. Li, H. F. Li, T. Iitaka, X. Zhong and Y. Xie, *Phys. Rev. B*, 2020, **101**, 7.
34. W. W. Cui, T. G. Bi, J. M. Shi, Y. W. Li, H. Y. Liu, E. Zurek and R. J. Hemley, *Phys. Rev. B*, 2020, **101**, 5.
35. T. Wang, M. Hirayama, T. Nomoto, T. Koretsune, R. Arita and J. A. Flores-Livas, Absence of conventional room temperature superconductivity at high pressure in carbon doped H₃S, 2021.
36. C. J. Pickard and R. J. Needs, *Phys. Rev. Lett.*, 2006, **97**, 4.
37. C. J. Pickard and R. J. Needs, *J. Phys. –Condes. Matter*, 2011, **23**, 23.
38. S. J. Clark, M. D. Segall, C. J. Pickard, P. J. Hasnip, M. J. Probert, K. Refson and M. C. Payne, *Z. Kristall.*, 2005, **220**, 567–570.
39. J. P. Perdew, K. Burke and M. Ernzerhof, *Phys. Rev. Lett.*, 1996, **77**, 3865.
40. Kresse and Furthmuller, *Physical review. B, Condensed matter*, 1996, **54**, 11169–11186.
41. G. Kresse and D. Joubert, *Phys. Rev. B*, 1999, **59**, 1758–1775.
42. D. J. Chadi, *Phys. Rev. B*, 1977, **16**, 1746.
43. P. Giannozzi, S. Baroni, N. Bonini, M. Calandra, R. Car, C. Cavazzoni, D. Ceresoli, G. L. Chiarotti, M. Cococcioni, I. Dabo, A. Dal Corso, S. de Gironcoli, S. Fabris, G. Fratesi, R. Gebauer, U. Gerstmann, C. Gougousis, A. Kokalj, M. Lazzeri, L. Martin-Samos, N. Marzari, F. Mauri, R. Mazzarello, S. Paolini, A. Pasquarello, L. Paulatto, C. Sbraccia, S. Scandolo, G. Sclauzero, A. P. Seitsonen, A. Smogunov, P. Umari and R. M. Wentzcovitch, *J. Phys. –Condes. Matter*, 2009, **21**, 19.
44. W. L. McMillan, *Physical Review*, 1968, **167**, 331.
45. P. B. Allen and R. C. Dynes, *Phys. Rev. B*, 1975, **12**, 905–922.
46. G. M. Eliashberg, *Sov Phys JETP*, 1960, **11**:3, 696–702.
47. G. Y. Gao, A. R. Oganov, Y. M. Ma, H. Wang, P. F. Li, Y. W. Li, T. Iitaka and G. T. Zou, *J. Chem. Phys.*, 2010, **133**, 5.
48. P. D. Ownby, X. Yang and J. Liu, 1992, **75**, 1876–1883.
49. H. Luo, R. G. Greene and A. L. Ruoff, *Phys. Rev. Lett.*, 1993, **71**, 2943–2946.
50. C. J. Pickard and R. J. Needs, *Nat. Phys.*, 2007, **3**, 473–476.